Cardiovascular Engineering and Technology, Vol. 10, No. 1, March 2019 *(© 2018)* pp. 124–135
https://doi.org/10.1007/s13239-018-00386-y

Reversed Auxiliary Flow to Reduce Embolism Risk During TAVI: A Computational Simulation and Experimental Study

MICHELE CONTI,[1] STIJN VANDENBERGHE,[2] STEFANIA MARCONI,[1] ENRICO FERRARI,[2] RODRIGO M. ROMAROWSKI,[4] SIMONE MORGANTI,[3] FERDINANDO AURICCHIO,[1] and STEFANOS DEMERTZIS[2]

[1]Department of Civil Engineering and Architecture, University of Pavia, Via Ferrata 3, 27100 Pavia, Italy; [2]Department of Cardiac Surgery, Cardiocentro Ticino, Lugano, Switzerland; [3]Department of Electrical, Computer, and Biomedical Engineering, University of Pavia, Pavia, Italy; and [4]3D and Computer Simulation Laboratory, IRCCS Policlinico San Donato, San Donato Milanese, Italy

(Received 23 February 2018; accepted 11 October 2018; published online 16 October 2018)

Associate Editor Dr. Ajit P. Yoganathan and Dr. Patrick Segers oversaw the review of this article.

Abstract
Introduction—Endovascular treatments, such as transcatheter aortic valve implantation (TAVI), carry a risk of embolization due to debris dislodgement during various procedural steps. Although embolic filters are already available and marketed, mechanisms underlying cerebral embolism still need to be elucidated in order to further reduce cerebrovascular events.
Methods—We propose an experimental framework with an in silico duplicate allowing release of particles at the level of the aortic valve and their subsequent capture in the supra-aortic branches, simulating embolization under constant inflow and controlled hemodynamic conditions. The effect of a simple flow modulation, consisting of an auxiliary constant flow *via* the right subclavian artery (RSA), on the amount of particle entering the brachiocephalic trunk was investigated. Preliminary computational fluid dynamics (CFD) simulations were performed in order to assess the minimum retrograde flow-rate from RSA required to deviate particles.
Results—Our results show that a constant reversed auxiliary flow of 0.5 L/min from the RSA under a constant inflow of 4 L/min from the ascending aorta is able to protect the brachiocephalic trunk from particle embolisms. Both computational and experimental results also demonstrate that the distribution of the bulk flow dictates the distribution of the particles along the aortic branches. This effect has also shown to be independent of release location and flow rate.
Conclusions—The present study confirms that the integration of *in vitro* experiments and in silico analyses allows designing and benchmarking novel solutions for cerebral embolic protection during TAVI such as the proposed embo-deviation technique based on an auxiliary retrograde flow from the right subclavian artery.

Keywords—Computational fluid dynamics, Aorta, Cerebral embolization, Transcatheter aortic valve implantation.

LIST OF SYMBOLS

AA	Ascending aorta
BCT	Brachiocephalic trunk
CRA	Cranial circulation
CAU	Caudal circulation
CFD	Computational fluid dynamics
DA	Descending aorta
LCCA	Left common carotid artery
LSA	Left subclavian artery
RCCA	Right common carotid artery
RSA	Right subclavian artery
TAVI	Transcatheter aortic valve implantation

INTRODUCTION

Aortic valve stenosis (AS) is a common disease of elderly patients, and it is constantly increasing following the progression of the life expectancy and the ageing of the population in Western countries.[34] During the last decade, Transcatheter Aortic Valve Implantation (TAVI) has become a valid alternative to standard surgery for the treatment of symptomatic AS in high-risk patients.[22] The procedure is based on the endovascular positioning and deployment of biological

Address correspondence to Michele Conti, Department of Civil Engineering and Architecture, University of Pavia, Via Ferrata 3, 27100 Pavia, Italy. Electronic mail: michele.conti@unipv.it

valve prosthesis, sewed into stent-like metallic frames, inside the native aortic valve. Since its first appearance, different models of TAVI devices and procedures have become available.[24]

Stroke is a risk of most cardiac surgical procedures[5] and a risk of TAVI as well: the position paper on TAVI elaborated by the European Society of Cardiology (ESC) and the European Association for Cardio-Thoracic Surgery (EACTS) acknowledges a (clinically evident) stroke rate between 3 and 9% for transfemoral TAVI and 0–6% for transapical TAVI.[44] Even more prevalent but more difficult to assess is the occurrence of sub-clinical brain lesions due to micro-emboli released during the procedure: clinically silent but morphologically detectable cerebral perfusion deficits occur in 84% of patients undergoing TAVI.[19] Even if the potential impact of these lesions to the neurocognitive function in the long term remains unknown, these numbers are worrisome. The relatively high stroke rate was re-confirmed in a more recent paper[33] reporting 9% of stroke after TAVI, of which more than 50% occurred within the first 24 hours. The overall incidence of cerebrovascular events complicating TAVI in the German Registry was 3.2%,[49] while other randomized trials have reported an incidence of stroke post TAVI ranging from 0.6 to 6%.[11,47]

Several devices aiming at capturing or deflecting embolic material during TAVI have been developed.[7,14,30,32] Unfortunately, such devices are not able to completely prevent cerebral micro-emboli or new transient ischemic lesions, as evaluated by cerebral diffusion-weighted magnetic resonance imaging.[38] Consequently, there is still room for a better understanding of embolism mechanisms to devise methods that could provide more brain vessels protection and prevent new lesions.[16]

The present study aims at modeling embolism during TAVI by *in vitro* experiments in parallel with computer simulations. An *in vitro* mock-circulatory loop is equipped to release particles in the aortic annulus and recapture them distally in order to quantify the emboli distribution along the supra-aortic branches under different hemodynamic conditions. Computational fluid dynamics (CFD) simulations were used to investigate a potential solution based on flow modulation at the level of the supra-aortic vessels to protect the cerebral circulation during TAVI. The required amount of flow injected from the right subclavian artery (RSA) was explored in a virtual manner prior to confirming this approach in bench tests. The proposed embo-deviation approach is grounded on the outcomes reported by Hedayati *et al.*,[17] who showed that an axillary artery cannulation for cardio-pulmonary bypass is cerebroprotective in a canine model: the altered blood-flow patterns during axillary cannulation induce retrograde brachiocephalic flow and competing intracerebral collateral blood flow able to deflect emboli from the ascending aorta and arch towards the descending aorta, potentially decreasing the incidence of stroke. Similar indications about the flow pattern reshaping were also reported by Demertzis *et al.*,[10] who were able to visualize the aortic flow pattern due to the right axillary artery cannulation, used in cardiac surgery, under conditions of either full or partial circulatory support.

METHODS

A mock circulatory loop where particles, representing emboli, are released and captured under controlled hemodynamic conditions was constructed. The setup is composed of the following parts: 1) aortic model; 2) centrifugal flow pump; 3) reservoir; 4) data acquisition system to monitor flow rates and pressures; 5) injection system to release the particles in the circuit; 6) filtering system to capture the released particles; 7) needle valves to adjust flow-split and mean pressure of the circuit. In the following, each component is discussed.

Aortic Model

An idealized model of the aortic arch and descending aorta using the CAD design software SolidWorks v. 24 (Dassault Systèmes, Velizy, France) was designed. Such a model, depicted in Fig. 1, resembles an average healthy aortic arch anatomy according to literature.[20] The CAD model was then exported in stereolithographic format (.stl) to create a 3D-printed physical model by a commercial high-resolution stereolithographic 3D printer (Form 2, Formlabs Inc., USA). The wall thickness of the model is variable (from 0.75 to 4 mm) (see Fig. 1) to achieve a sufficient resistance for handling and pressurization, i.e., an average 100 mmHg. Resin Clear—RS-F2-GPCL-02—was used to print the model with a layer thickness of 100 μm, ensuring high transparency in wet conditions; transparency is indeed a mandatory feature for our analysis because images and videos of the model are captured during the particles' release to have a qualitative indication of their path and distribution along the aortic arch. The model is rigid, a necessary working condition to be counterparted by CFD analysis.

Mock Circulatory Loop

The aortic model was connected with ½″ tubes (Raumedic ECC-SIK; Rehau, Isernhagen, Germany)

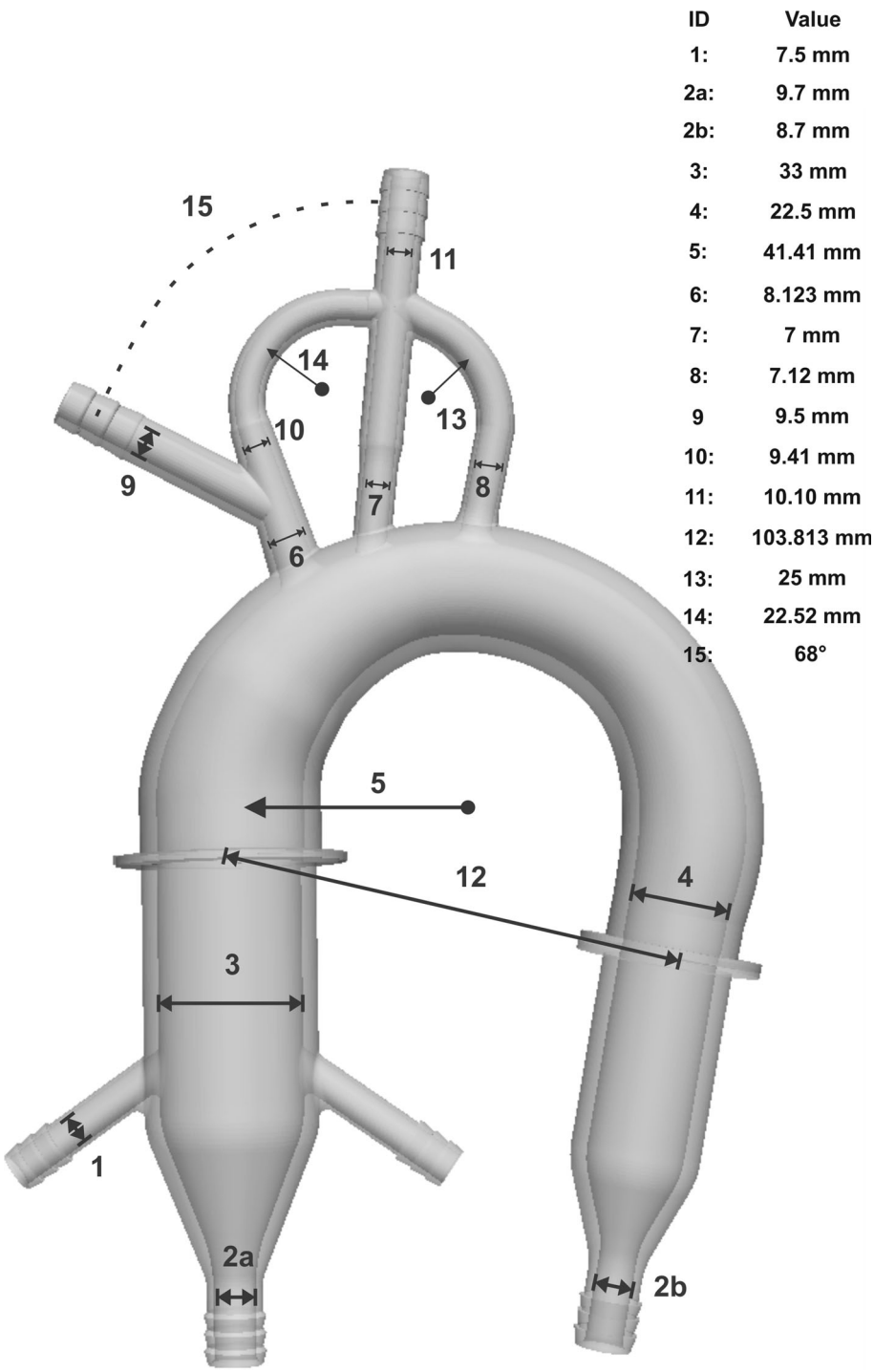

FIGURE 1. Aortic model and its main dimensions. IDs of the major vessels are as follows: 3—AA, 4—DA, 6—BCT, 9—RSA, 10—RCCA, 7—LCCA and 8—LSA.

to the hydraulic circuit (see Fig. 2a), filled with water at room temperature and driven by a centrifugal pump (Medtronic Bioconsole BIO-MEDICUS 550, Minneapolis, MN, USA), imposing constant inflow, which is measured by a clamp-on flowmeter (SonoTT Clamp-On transducer, Em-Tec GmbH, Finning, Germany) positioned at the inlet of the aortic model. The supra-aortic branches were distally merged to one vessel in order to enable flow quantification only in two major directions: cranial (CRA), i.e., towards the cerebral circulation; caudal (CAU), i.e., towards the descending aorta. Although this choice implies limitations, it

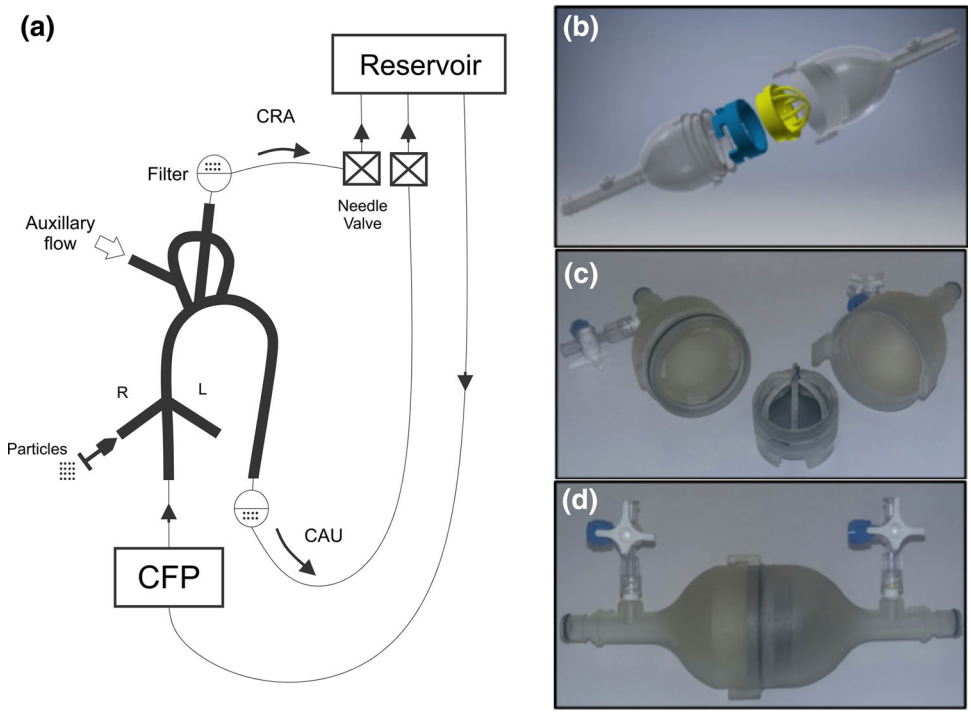

FIGURE 2. (a) Schematic representation of the mock circulatory loop; (b) assembly of CAD drawings of the filter basket; (c) 3D printed components of the filter basket assembled; (d) to be plugged in the circuit. CFP—centrifugal pump; CRA—cranial direction; CAU—caudal direction; R—right; L—left.

simplifies the experimental activities because it allows: (1) easy tuning of the CRA/CAU flow split; (2) using one filter to capture the corresponding particles, avoiding smaller filters which can be more easily clogged up by few particles. Consequently, each major branch contains a filter for capturing particles and a downstream needle valve to set the hydraulic resistance and thereby the CRA/CAU flow split ratio of 35/65, respectively, according to literature.[8] As working assumption, this ratio has been kept constant also when auxiliary flow was added from the RSA. This flow split is measured by switching the flowmeter transducer from the inlet to the CAU outlet. The outlet tubes and the inlet tube of the pump are connected to a 5 L reservoir, mounted on a pole to enable the adjustment of the working pressure *via* reservoir height. The working pressure is defined as the average of the pressures read at the level of the two filters by pressure sensors (Micro Switch Pressure Sensor 40PC Series, Honeywell, Freeport, IL, USA) connected to a NI DAQ USB-6210 board (National Instruments, Austin, TX, USA).

According to Bachman *et al.*,[4] we have adopted Amberlite particles as embolic models. A bolus of 0.50 g of neutrally-buoyant particles with a harmonic mean size of 0.550–0.750 mm (Amberlite IRA-96 free base, Sigma-Aldrich) is injected at the level of the aortic root. The selected size range of the particles includes the smallest size adopted by Bushi *et al.*[6] (i.e., 0.6 mm), who evaluated the behaviour of 1.6 and 3.2 mm particles as well. The dimension of our particles resembles also the smallest size of amorphous calcified debris reported by the study of Van Mieghem *et al.*[46]

The speed of particle injection is controlled by a syringe pump (NE-4000 Two Channel Syringe Pump Multi-Phaser, Syringe Pump, USA) that drives the particle bolus release in the aortic model in a short amount of time, i.e., between 4 and 5 s, resembling the time required to deploy a valvular prosthesis. The released particles are captured by two filter baskets, which were realized using the same stereolithographic 3D-printer and the same material of the aortic model; in this case, a higher layer resolution of 50 μm due to the finer details of the design is used. As illustrated by Fig. 2b, the filter was designed (Autodesk Inventor 2017 Student Edition, Autodesk Inc., San Rafael, California, USA) to facilitate its assembly, being composed by a case holding a basket where a stockings net (100% polyamide–22 dtex), with an approximate pore size of 0.1 mm, was embedded; the plug-and-play design of the filter allows repeating the experiment in a fast and efficient manner. Each part of the filter (see Fig. 2c) incorporates luer lock connectors to plug the pressure sensors; we ensured a minimum pressure gradient of 0.1 mmHg to minimize its impact on the

experiments. After each experiment, the net containing the captured particles was carefully removed from the basket, dried and weighed using an electronic balance with a 0.01 g readability (GandG GmbH, Germany) to evaluate the particle distribution as function of the controlled flow-pressure conditions.[6]

Computational Fluid Dynamics

The previously described aortic CAD model was also processed to generate a CFD-suitable domain. Volume meshing of the geometry was performed with VMTK software suite[1] that resulted in a mesh of 1.05 million elements following a sensitivity analysis for the velocity field, which is the main contributor to particle tracking. The granularity is on the range of similar experiments within the thoracic aorta.[23,43]

As for the boundary conditions, on the section representing the aortic root, a constant flow rate of 4 L/min was prescribed using a Dirichlet boundary condition and a plug profile. On the outflow sections, we prescribed the flow split conditions adopted for the *in vitro* experiments: 35% of the outflow in the cranial direction and 65% in the caudal direction. To do so, Dirichlet outlet with a flat velocity profile was used in the CRA boundary, whereas stress-free boundary condition was used at CAU outlet section. In order to find the inflow threshold from the RSA that would refrain particles from entering into the cerebral circulation through the right common carotid artery (RCCA), a flat velocity profile ranging from 0.0 to 0.5 L/min, with steps of 0.1 L/min, was plugged in the RSA. Cranial flow split was modified accordingly to be 35% of the inflow to the domain also in this case.

To acknowledge potential differences with a pulsatile flow model, we performed two simulations with an ascending aortic flow wave extracted from Morbiducci *et al.*[26] and then scaled to match the 4 L/min flow used in the steady counterpart. In one of them, no flow was injected from the RSA, whereas the other one had the same auxiliary inflow of 0.5 L/min that was used in the steady model. Boundary conditions are imposed according to the approach proposed for the steady case. Simulations were run for 6 cycles in order to achieve periodicity and avoid initial transitory states and the timestep used was 0.001 s in order to ensure a Courant-Friedrichs-Lewy (CFL) number below 1 along the entire cardiac cycle.[25]

In the simulations, walls were assumed as rigid with a no-slip boundary condition. Blood was treated as Newtonian with a viscosity of 0.0035 Pa s and a density of 1060 kg/m^3. LifeV finite element library for solving the Navier–Stokes equations was used in four AMD Opteron 6272 processors to run the simulations.[35] Numerically, these equations are discretized in time using a second-order Backward Differentiation Formula (BDF2)[36] and in space using inf–sup stable elements such as P1Bubble-P1 for the velocity and pressure fields, respectively. The system is first left-preconditioned and then solved with the GMRES iterative method,[40] tolerances for the continuity and velocity equations were set to 10^{-5}. Due to the laminar nature of flow at these low Reynolds numbers, no turbulence model was used and only streamline diffusion was used for stabilizing the highest velocities within the domain.[15]

Point-wise velocity field computed by CFD during the last simulated cycle was post-processed with Paraview (Kitware, FR) where a source of massless particle was placed in the corresponding inflow as proposed in the *in vitro* counterpart. In the unsteady simulation, the bolus was released at the beginning of the systole ($t = 0$ s) and five cycles were tracked after the injection of the bolus to give all the particles time to exit the domain (i.e., the wash-out lapse for all the particles). Particles were traced in order to: (a) account for the particle split between the CAU and CRA circulations and (b) to quantify the percentage of released particles entering the brachiocephalic trunk (BCT).

Experimental Set

We ran three series of the experiments. The first one aimed at investigating the impact inflow rates (3 or 4 L/min) and release side (right or left lateral aortic annulus) on the particles' distribution, while in the second series, with the same aim, we evaluated the impact of changing the CRA/CAU. In the first series, five repetitions were performed for each combination of conditions to assess reproducibility of this test and measuring method. Both test series are performed without auxiliary flow from the RSA.

Finally, based on the steady CFD simulation results, we performed the particle injection when 0.5 L/min auxiliary flow from the RSA is active to confirm that it would actually abstain the particles to enter the cranial circulation through the RCCA. According to the results of the previous tests detailed in the next section, three repetitions were performed for the last series because previous tests showed the good repeatability of the results and particles were injected from the right side because both access sides are equivalent for our purposes. The inflow from the aortic root was 4 L/min.

TABLE 1. Measurement of the particle split as function of different access side and inlet flow rate.

		Flow split		Particle split	
Access	Inlet flow (L/min)	CRA (%)	CAU (%)	CRA (%)	CAU (%)
Right access	3.4 (± 0.02)	31 (± 2.1)	69 (± 2.1)	37 (± 3.6)	62 (2.6)
	4.1 (± 0.1)	33 (± 1.4)	67 (± 1.4)	33 (± 3.0)	67 (± 3.0)
Left access	3.2 (± 0.1)	36 (± 1.1)	64 (± 1.1)	35 (± 2.3)	65 (± 2.3)
	4.3 (± 0.1)	33 (± 1.1)	67 (± 1.1)	32 (± 5.7)	68 (± 5.7)

The results are reported as mean and standard deviation (STD) of the five repetitions performed for each case under investigation.

RESULTS

The results of the first series of experiments are reported as mean and standard deviation in Table 1. From the right aortic annulus release side, given an inflow of 3.4 ± 0.02 L/min and a CRA/CAU flow split ratio of 31 ± 2.1/69 ± 2.1, we measured a CRA/CAU particle distribution of 37 ± 3.6/62 ± 2.6; while given an inflow of 4.1 ± 0.1 L/min and a CRA/CAU flow split of 33 ± 1.4/67 ± 1.4, we measured a CRA/CAU particle distribution of 33 ± 3.0/67 ± 3.0. From the left release side, given an inflow of 3.2 ± 0.1 L/min and a CRA/CAU flow split of 36 ± 1.1/64 ± 1.1, we measured a CRA/CAU particle distribution of 35 ± 2.3/65 ± 2.3; while given an inflow of 4.3 ± 0.1 L/min and a CRA/CAU flow split of 33 ± 1.1/67 ± 1.1, we measured a CRA/CAU particle distribution of 32 ± 5.7/68 ± 5.7. All the released particles were successfully captured, as the pre-release weight equaled the post-capture weight for each experiment. The standard deviation for the repeated measures of particle collection was < 6% overall; this result suggests that the release and catch method is sufficiently consistent to draw conclusions for future testing of embolic protection devices and risk of stroke when a large number of particles is used because our counting method is based on particles' weighting, which fails in accuracy when only few particles are considered. Our results demonstrated that the distribution of the bulk flow dictates the distribution of the particles along the aortic branches, which seems to be independent of access side and flow rate. In fact, to corroborate this finding we enforced in the second series of experiments more extreme conditions of the flow split, as shown in Table 2: under an inflow of 4 L/min, given a CRA/CAU flow split of 50/50, we measured a CRA/CAU particles' distribution of 50/50, while given a CRA/CAU flow split of 19/81, we measured a CRA/CAU particles' distribution of 18/82.

The results of the CFD simulations reported in Fig. 3 suggest that an RSA auxiliary flow of 0.5 L/min is enough to deviate the injected particles and to avoid their entrance in the brachiocephalic trunk when a steady inflow is considered. Figure 4 confirms this phenomenon in the *in vitro* setup, where the same auxiliary flow from RSA refrains the particles to enter the BCT. This is mostly caused by the division of the inflow jet: part of the auxiliary flow goes cranially, while the remaining part goes retrograde to the arch creating a barrier for the particles, which unfortunately are still able to run through the LCCA. The current setup does not allow counting the subdivisions of the particles along the three supra-aortic branches so we are not able to assess if the auxiliary flow reduces or even increases the amount of particles running through the LCA. Videos 1 and Videos 2 show the release of the particles without and with the auxiliary flow, respectively. As reported in Table 3, the use of the auxiliary flow reduces the number of particles diverting towards the cranial direction (− 5%); in fact, we measure a CRA/CAU particle split of 28 ± 2.0/72 ± 2.0 which is similar to the control condition, with no auxiliary flow, i.e., 33 ± 3.1/67 ± 3.1. Similar indications are obtained by in silico simulations that confirm a reduction of CRA particles (− 10%) when auxiliary flow is on. Despite both approaches indicate the same trend about particle split, there is a difference in magnitude, suggesting that the treatment of particles in the CFD studies, injected as massless particles, does not necessarily represent the *in vitro* experiment, while it is certainly valid for particle image velocimetry where the particles are much smaller (< 100 μm).[37]

Unsteady simulation results with no inflow from the RSA confirmed that the particle split followed the flow split (i.e., 35 CRA/65 CAU). However, when we added the 0.5 L/min auxiliary flow, we had more particles

TABLE 2. Measurement of the particle split as function of different flow split.

	Flow split		Particle split	
Inlet flow (L/min)	CRA (%)	CAU (%)	CRA (%)	CAU (%)
4.03	50	50	50	50
3.98	19	81	18	82

Only one experiment is performed for each case.

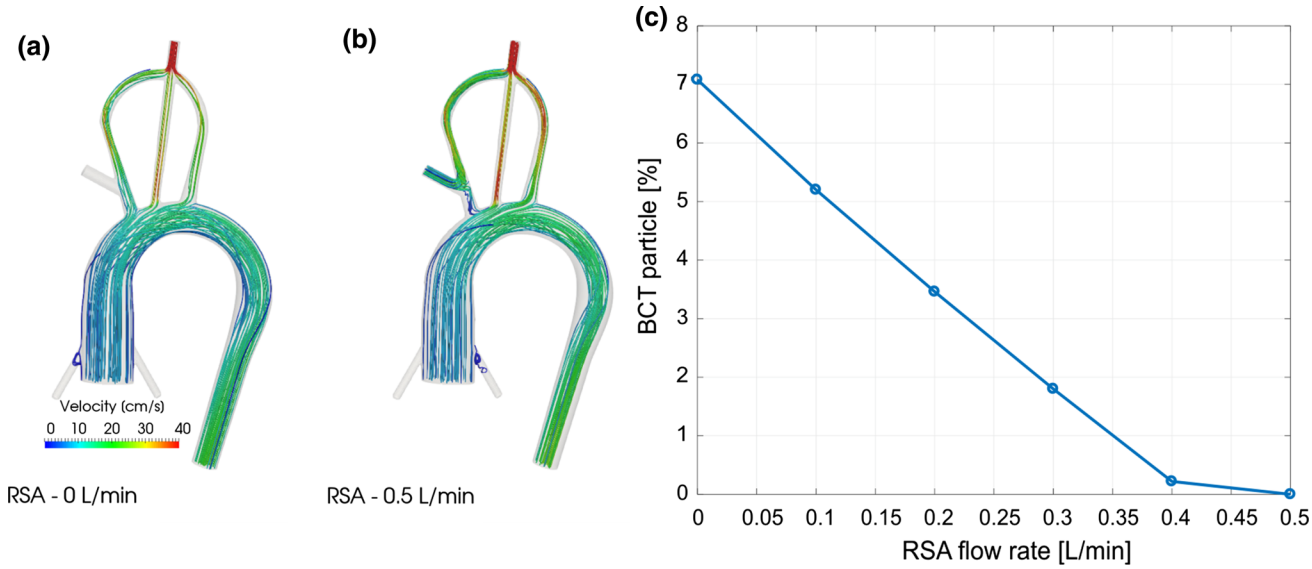

FIGURE 3. Results of numerical simulations: (a) streamlines resulting from CFD analysis when RSA auxiliary flow is not activated; (b) streamlines resulting from CFD analysis accounting for 0.5 L/min RSA auxiliary flow; (c) percentage of injected particle running through brachio-cephalic trunk (BCT) as function of RSA flow rate, resulting from particle tracking analysis.

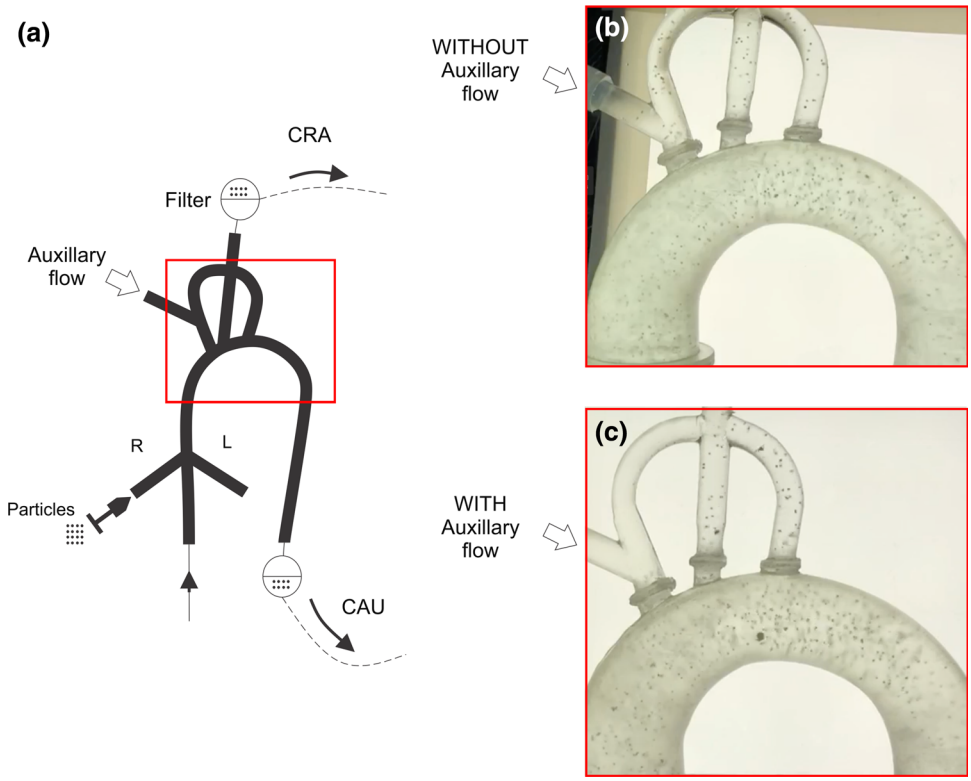

FIGURE 4. (a) Schematic representation of the mock circulatory loop with red box highlighting the region depicted in (b) showing the case when particles are released without auxiliary flow from right subclavian artery (RSA) and (c) when the auxiliary flow is present.

going to the CAU circulation and the ratio became 28 CRA/72 CAU. This demonstrated that the inflow jet diverted debris to the descending aorta. In detail, particle split changed between the steady and unsteady simulation as follows: BCT + 4%, LCCA + 2%, LSA − 18% and CAU + 12%. Therefore, the auxil-

TABLE 3. Measurement of the particle split with and without auxiliary flow from right subclavian artery.

		Flow split		Particle distribution	
	Inlet flow (L/min)	CRA (%)	CAU (%)	CRA (%)	CAU (%)
Inlet: 4 L/min	4.02	35	65	34	66
RSA: 0 L/min	4.06	35	65	36	64
	4.01	35	65	30	70
	4.03 (± 0.03)	35	65	33 (± 3.1)	67 (± 3.1)
Inlet: 4 L/min	4.0	35	65	30	70
RSA: 0.5 L/min	4.0	35	65	28	72
	4.07	35	65	26	74
	4.04 (± 0.03)	35	65	28 (± 2.0)	72 (± 2.0)

Three repetitions are performed for each case; the results are reported as mean and standard deviation (STD) as well.

iary flow was not enough to divert all of the particles from reaching the BCT, which are still the 15% of the particles entering in the supra-aortic branches.

DISCUSSION

Intraoperative embolism during TAVI is still a controversial open issue and its impact on the prognosis of the treatment is relevant: patients suffering from stroke complicating TAVI showed up to ten-fold increase in-hospital mortality rates when compared to patients without stroke[42]; moreover, stroke is an independent predictor of 1-year mortality after TAVI in clinical practice.[50] Therefore, it is fundamental to try to prevent neurological event related to TAVI embolisms and design novel embo-protective solutions grounded on the analysis of the underlying mechanisms, benchmarked with reliable models.[39] Given these aims, a mock circulatory loop was constructed where a bolus of particles, modeling the emboli, was released and captured under controlled hemodynamics conditions. *In-vitro* experiments were counter parted by in silico analyses. In particular, we exploited the system to explore the use of an auxiliary flow from the RSA in order to avoid debris to enter the cerebral circulation. With CFD simulation support we tuned the right inflow value that would produce embo-deviation.

We developed a 3D printed aortic model connected to the mock circulatory loop where, under constant inflow and controlled pressure conditions, particles can be released at the level of the aortic root and captured in the main aortic branches. The present *in vitro* setup uses an idealized aortic model instead of a simplified Y-shaped phantom as analogue to an arterial bifurcation, as proposed in the work of Bushi *et al.*[6] Other *in vitro* studies dealing with analysis of cerebral embolisms modeled by release of particles are related to the intra-cranial circulation,[9,13] where the aorta is not explicitly included in the model. In this context, it is worth noting that, in the last years, there has been a growing interest for the application of computational tools simulating particle behavior in complex arterial networks (see for instance Mukherjee and Shadden[29]).

From the results of our *in vitro* experiments, we found that the particle distribution substantially follows the flow split. This result is consistent with the simulation results of Carr *et al.*[8] who used computed tomography (CT) scan derived models of the human aorta with branches for the head and computed the particles' behavior with diameter ranging from 0 to 4 mm, in increments of 250 μm. Similar findings were reported by Bushi *et al.*[6]: small (0.6 mm) and mid-sized (1.6 mm) particles entered into bifurcation daughter branches proportionally to the flow split.

When the auxiliary flow from RSA is active in the steady configuration, we observed a total embolic protection effect towards the BCT, while emboli were able to enter the LCCA.

Of note, the in silico support provided by the CFD simulation allowed us to find the hemodynamic condition required for diverting the particles in a very simple way, rather than running a series of *in vitro* experiments with increasing flows from the LSA, demonstrating to be a robust base to modify any geometrical and flow parameter before making changes in the experimental setup. The unsteady simulations had the goal to acknowledge the differences with the steady flow, which to the best of our knowledge is more realistic because of the rapid pacing during surgery. Results were significantly different to the steady analysis, showing that the same auxiliary flow did not reach total embo-deviation when flow is pulsatile. This was mostly due to the high instantaneous flow from the heart during systole. Further investigations are required to provide insight in such differences among various hemodynamic conditions since the lack of experimental results on this type of flow hinders an extensive comparison with *in vitro* data as has been done with the steady simulations.

From a more general point of view, the use of *in vitro* and computer-based methods allows to investigate realistic human aortic geometries. Even though we adopted an idealized 3D arch prototype, our geometrical model is more realistic than the aortic arch of an *in vivo* porcine model: pigs weighing more than 50 kg have aortic dimensions comparable to humans but the branching anatomy of the porcine arch is characterized by a single brachiocephalic vessel from which both carotid arteries derive; furthermore, the second arch vessel is a separate left subclavian artery. This anatomical condition is seen in a rather low percentage of humans with the bovine arch anatomy and does not accurately represent average human vasculature. Certainly, *in vivo* animal models offer the possibility to test the device in an environment which extremely close to the surgical reality and remain the gold standard for device benchmarking prior clinical human trials.[18]

Study Limitations

One of the main limitations of the present study is that we used water at room temperature as blood analogue.[21,31] this was chosen for practical reasons to prevent clumping of the Amberlite particles, which would occur with a typical glycerin-mixture blood analog fluid.

In our study, we considered only spherical 0.550–0.750 mm particles, which can be catalogued as medium particles, although the emboli observed during cardiac interventions are of variable sizes and shapes (as well as having heterogeneous consistency and histological composition).[46] Van Mieghem *et al.*[46] used commercially available filters to capture and analyze, also histologically, the debris released during TAVI. Their findings indicate that the macroscopic captured material varied in size from 0.15 to 4.0 mm and consisted of: amorphous calcified material (size, 0.55–1.8 mm); valve tissue composed of loose connective tissue (size, 0.25–4.0 mm); thrombotic material intermixed with neutrophils (size, 0.15–2.0 mm). Subsequently, the same research group[45] investigated a larger cohort of patients reporting a broader range of particle size, (i.e., from 0.1 to 9.0 mm). Moreover, particle dynamics into blood stream are likely to vary if these issues are taken into consideration, which we disregarded for the sake of simplicity. Given these considerations, future studies should address analysis of various sizes of particles elucidating mechanisms of their distribution in the arterial tree, which are still a matter of debate. In fact, published *in vitro* results[6,9] showed that particle distribution, beyond its outlets-flow-ratios, is influenced by the particle-to-branch diameter-ratio with large particles preferentially entering into wider bifurcated branches. The results of Bushi are not confirmed by Carr *et al.*,[8] who hypothesized that this mismatch is due to the curvature of the aorta and pulsatile nature of aortic flow, coupled with inertial effects of the particles. We like to add that geometry and resulting lift and drag forces may play a role as well, further complicating detailed analyses. Moreover, we have adopted neutrally-buoyant particles although the impact of particle density on their distribution deserves further investigations. Indeed, no measured density values of different embolic particles are available in literature as stated by Fabbri *et al.*,[12] who have investigated the influence of microembolic particle size and density on travel trajectories in cerebral arteries only by computational modelling, selecting the hypothetical particle density with a pure comparison with blood density. The indication about debris density is also missing in the clinical studies addressing the cataloguing of particles released during TAVI.[46] Other *in vitro*[6,8] and *in silico*[9] studies have limited their investigation to a narrow range of densities and in most cases adopting the density of blood.

For the sake of simplicity, we did not consider pulsatile inflow and aortic compliance at this stage of the experiments. We consider this to be a significant limitation, however, constant flow comes close to the hemodynamic pattern created by rapid ventricular pacing, still widely used during TAVI, which leads to a significant reduction of the cardiac output during the valve delivery.

In our setup we are not explicitly accounting for the presence of both native and prosthetic valve; in this regard, it is worth remarking that the type of prosthesis has a limited impact on the risk of stroke.[2]

In our model the supra-aortic branches (BCT, LCCA and LSA) are distally merged; consequently, the experimental setup has only one filter in the CRA circulation and we were able only to evaluate the overall CRA/CAU particle distribution while the number of particles entering each supra-aortic branch is not measured. This analysis could be addressed by future improvement of the experimental set-up overcoming filtering and using alternative ways to detect and count the particles, such as Transcranial Doppler (TCD) ultrasound or by dedicated computational studies, which are more amenable for parametric studies.[8] The CRA/CAU flow ratio has been kept constant also when auxiliary flow was added from the RSA; this is an assumption to be further investigated in future studies. Finally, the use of rigid walls can be considered a further limitation, but according to the purpose of the study, the choice is specifically made to enable the integration of the *in vitro* setup with CFD analysis. Furthermore, with steady flow there is no benefit in applying a compliant wall model, and the

rigid wall hypothesis is considered valid in the most advanced computer-based simulations about cerebral embolism[27] while the impact of wall compliance on the embolic distribution along arterial circulation is still unknown. Despite the steady flow assumption seems reasonable because pulse pressure is damped during rapid ventricular pacing of TAVI,[48] further studies should include different hemodynamic conditions resembling the various stages of TAVI implant; at the same, further clinical data quantifying intra-operative aortic hemodynamics are necessary.

In the present study, we limited the use of CFD simulations to the assessment of optimal reversal flow from RSA, although its potentiality in the analysis of cerebral embolism is high as proved by the growing interest for the numerical simulations of particle behavior in complex arterial networks.[3,12,27,28,41] Following such a trend, future developments of the present study will account for a stronger integration of *in vitro* and in silico tools, based on the implementation of dedicated numerical algorithms able to model inertial dynamics of the particles, which we considered massless, a reasonable hypothesis given the size of the particles (0.5 mm) under investigation.[8] Lastly, the present study uses the weight as the method to evaluate particle destination according to similar previous studies.[6] This is a straightforward approach, which unfortunately becomes cumbersome in the simulation of an actual stroke induced by one or a few particles; in this case, *in vitro* studies have a limited efficacy while CFD-based approaches provide the ability to release and track numbered particles.

CONCLUSIONS

The present study tested a hypothetical alternative to intravascular filters to protect cerebral circulation from emboli released during endovascular procedures, such as TAVI, by a mock circulatory loop and computational simulations. Our model was used to analyze how particles split along the aortic branches and evaluate possible solutions to deviate their path from cerebral circulation. For the chosen configuration, our results show that a constant reversed auxiliary flow of 0.5 L/min from RSA under a constant inflow of 4 L/min from the ascending aorta is able to protect the brachiocephalic trunk from embolisms although the presented auxiliary flow is not a final therapeutic product but just a simple test to evaluate the potential of flow deviation approach.

The present study addresses the need of investigating the mechanisms underlying TAVI-related cerebral embolism,[39] encouraging the design of novel approaches overcoming the use of intravascular filters to protect cerebral circulation from emboli released during TAVI.

ELECTRONIC SUPPLEMENTARY MATERIAL

The online version of this article (https://doi.org/10.1007/s13239-018-00386-y) contains supplementary material, which is available to authorized users.

ACKNOWLEDGMENTS

The authors acknowledge Eng. M. Stochino and Eng. G. Fiorani for their support with the experimental data collection.

FUNDING

The present study was partially funded by a 2016 Research Grant of European Society of Cardiology (ESC).

CONFLICT OF INTEREST

Michele Conti declares that he has no conflict of interest. Stijn Vandenberghe declares that he has no conflict of interest. Stefania Marconi declares that she has no conflict of interest. Enrico Ferrari declares that he has no conflict of interest. Rodrigo Romarowski declares that he has no conflict of interest. Simone Morganti declares that he has no conflict of interest. Ferdinando Auricchio declares that he has no conflict of interest. Stefanos Demertzis declares that he has no conflict of interest.

ETHICAL APPROVAL

This article does not contain any studies with human participants or animals performed by any of the authors.

REFERENCES

[1]Antiga, L., M. Piccinelli, L. Botti, B. Ene-Iordache, A. Remuzzi, and D. A. Steinman. An image-based modeling framework for patient-specific computational hemodynamics. *Med. Biol. Eng. Compu.* 46:1097–1112, 2008.

[2]Athappan, G., R. D. Gajulapalli, P. Sengodan, A. Bhardwaj, S. G. Ellis, L. Svensson, E. M. Tuzcu, and S. R. Kapadia. Influence of transcatheter aortic valve replacement strategy and valve design on stroke after transcatheter aortic valve replacement: a meta-analysis and

systematic review of literature. *J. Am. Coll. Cardiol.* 63(20):2101–2110, 2014.
[3]Aycock, K. I., R. L. Campbell, K. B. Manning, and B. A. Craven. A resolved two-way coupled CFD/6-DOF approach for predicting embolus transport and the embolus-trapping efficiency of IVC filters. *Biomech. Model. Mechanobiol.* 16(3):851–869, 2017.
[4]Bachman, T. N., J. K. Bhama, J. Verkaik, S. Vandenberghe, R. L. Kormos, and J. F. Antaki. In vitro evaluation of ventricular cannulation for rotodynamic cardiac assist devices. *Cardiovasc. Eng. Technol.* 2:203, 2011.
[5]Bucerius, J., J. F. Gummert, M. A. Borger, T. Walther, N. Doll, J. F. Onnasch, *et al.* Stroke after cardiac surgery: a risk factor analysis of 16,184 consecutive adult patients. *Ann. Thorac. Surg.* 75(2):472–478, 2003.
[6]Bushi, D., Y. Grad, S. Einav, O. Yodfat, B. Nishri, and D. Tanne. Hemodynamic evaluation of embolic trajectory in an arterial bifurcation. *Stroke* 36:2696–2700, 2005.
[7]Carpenter, J. P., J. T. Carpenter, A. Tellez, J. G. Webb, G. H. Yi, and J. F. Granada. A percutaneous aortic device for cerebral embolic protection during cardiovascular intervention. *J. Vasc. Surg.* 54:174–181, 2011.
[8]Carr, I. A., N. Nemoto, R. S. Schwartz, and S. C. Shadden. Size-dependent predilections of cardiogenic embolic transport. *Am. J. Physiol. Heart Circ. Physiol.* 305:H732–H739, 2013.
[9]Chung, E. M., J. P. Hague, M. A. Chanrion, K. V. Ramnarine, E. Katsogridakis, and D. H. Evans. Embolus trajectory through a physical replica of the major cerebral arteries. *Stroke* 41:647–652, 2010.
[10]Demertzis, S., H. Tevaearai, T. Carrel, and S. Vandenberghe. Aortic flow patterns resulting from right axillary artery cannulation. *Interact. Cardiovasc. Thorac. Surg.* 12:973–977, 2011.
[11]Eltchaninoff, H., A. Prat, M. Gilard, A. Leguerrier, D. Blanchard, G. Fournial, B. Iung, P. Donzeau-Gouge, C. Tribouilloy, J. L. Debrux, and A. Pavie. Transcatheter aortic valve implantation: early results of the FRANCE (FRench Aortic National CoreValve and Edwards) registry. *Eur. Heart J.* 32:191–197, 2010.
[12]Fabbri, D., Q. Long, S. Das, and M. Pinelli. Computational modelling of emboli travel trajectories in cerebral arteries: influence of microembolic particle size and density. *Biomech. Model. Mechanobiol.* 13(2):289–302, 2014.
[13]Fahy, P., F. Malone, E. McCarthy, P. McCarthy, J. Thornton, P. Brennan, A. O'Hare, S. Looby, S. Sultan, N. Hynes, and L. Morris. An in vitro evaluation of emboli trajectories within a three-dimensional physical model of the circle of willis under cerebral blood flow conditions. *Ann. Biomed. Eng.* 43:2265–2278, 2015.
[14]Gallo, M., A. Putzu, M. Conti, G. Pedrazzini, S. Demertzis, and E. Ferrari. Embolic protection devices for transcatheter aortic valve replacement. *Eur. J. Cardiothorac. Surg.* 53:1118–1126, 2018.
[15]Hansbo, P., and A. Szepessy. A velocity–pressure streamline diffusion finite element method for the incompressible Navier–Stokes equations. *Comput. Methods Appl. Mech. Eng.* 84(2):175–192, 1990.
[16]Haussig, S., N. Mangner, M. G. Dwyer, L. Lehmkuhl, C. Lücke, F. Woitek, D. M. Holzhey, F. W. Mohr, M. Gutberlet, R. Zivadinov, and G. Schuler. Effect of a cerebral protection device on brain lesions following transcatheter aortic valve implantation in patients with severe aortic stenosis: the CLEAN-TAVI randomized clinical trial. *JAMA* 316:592–601, 2016.
[17]Hedayati, N., J. T. Sherwood, S. J. Schomisch, J. L. Carino, and A. H. Markowitz. Axillary artery cannulation for cardiopulmonary bypass reduces cerebral microemboli. *J. Thorac. Cardiovasc. Surg.* 128:386–390, 2004.
[18]Hoekstra, A. G., E. van Bavel, M. Siebes, F. Gijsen, and L. Geris. Virtual physiological human 2016: translating the virtual physiological human to the clinic. *Interface Focus* 8:20170067, 2016.
[19]Kahlert, P., S. C. Knipp, M. Schlamann, M. Thielmann, F. Al-Rashid, M. Weber, U. Johansson, D. Wendt, H. G. Jakob, M. Forsting, and S. Sack. Silent and apparent cerebral ischemia after percutaneous transfemoral aortic valve implantation. *Circulation* 121:870–878, 2010.
[20]Kahraman, H., M. Ozaydin, E. Varol, S. M. Aslan, A. Dogan, A. Altinbas, M. Demir, O. Gedikli, G. Acar, and O. Ergene. The diameters of the aorta and its major branches in patients with isolated coronary artery ectasia. *Tex. Heart Inst. J.* 33:463–468, 2006.
[21]Krüger, T., A. Grigoraviciute, K. Veseli, D. Schibilsky, H. P. Wendel, W. Schneider, and C. Schlensak. Elastic properties of the young aorta: ex vivo perfusion experiments in a porcine model. *Eur. J. Cardiothorac. Surg.* 48:221–227, 2014.
[22]Ludman, P. F., N. Moat, M. A. de Belder, D. J. Blackman, A. Duncan, W. Banya, P. A. MacCarthy, D. Cunningham, O. Wendler, D. Marlee, and D. Hildick-Smith. Transcatheter aortic valve implantation in the UK: temporal trends, predictors of outcome and 6 year follow up: a report from the UK TAVI Registry 2007 to 2012. *Circulation* 131(13):1181–1190, 2015.
[23]Marrocco-Trischitta, M. M., T. M. van Bakel, R. M. Romarowski, H. W. de Beaufort, M. Conti, J. A. van Herwaarden, F. L. Moll, F. Auricchio, and S. Trimarchi. The Modified Arch Landing Areas Nomenclature (MALAN) improves prediction of stent graft displacement forces: proof of concept by computational fluid dynamics modelling. *Eur. J. Vasc. Endovasc. Surg.* 55(4):584–592, 2018.
[24]Masson, J. B., J. Kovac, G. Schuler, J. Ye, A. Cheung, S. Kapadia, M. E. Tuzcu, S. Kodali, M. B. Leon, and J. G. Webb. Transcatheter aortic valve implantation: review of the nature, management, and avoidance of procedural complications. *JACC Cardiovasc. Interv.* 2:811–820, 2009.
[25]Morbiducci, U., R. Ponzini, D. Gallo, C. Bignardi, and G. Rizzo. Inflow boundary conditions for image-based computational hemodynamics: impact of idealized versus measured velocity profiles in the human aorta. *J. Biomech.* 46(1):102–109, 2013.
[26]Morbiducci, U., R. Ponzini, G. Rizzo, M. Cadioli, A. Esposito, F. De Cobelli, A. Del Maschio, F. M. Montevecchi, and A. Redaelli. In vivo quantification of helical blood flow in human aorta by time-resolved three-dimensional cine phase contrast magnetic resonance imaging. *Ann. Biomed. Eng.* 37(3):516, 2009.
[27]Mukherjee, D., N. D. Jani, K. Selvaganesan, C. L. Weng, and S. C. Shadden. Computational assessment of the relation between embolism source and embolus distribution to the circle of willis for improved understanding of stroke etiology. *J. Biomech. Eng.* 138(8):081008, 2016.
[28]Mukherjee, D., J. Padilla, and S. C. Shadden. Numerical investigation of fluid–particle interactions for embolic stroke. *Theoret. Comput. Fluid Dyn.* 30(1–2):23–39, 2016.
[29]Mukherjee, D., and S. C. Shadden. Inertial particle dynamics in large artery flows—implications for modeling arterial embolisms. *J. Biomech.* 52:155–164, 2017.

[30]Naber, C. K., A. Ghanem, A. A. Abizaid, A. Wolf, J. M. Sinning, N. Werner, G. Nickenig, T. Schmitz, and E. Grube. First-in-man use of a novel embolic protection device for patients undergoing transcatheter aortic valve implantation. *EuroIntervention*. 8:43–50, 2012.

[31]Nauta, F. J., M. Conti, S. Marconi, A. V. Kamman, G. Alaimo, S. Morganti, A. Ferrara, J. A. van Herwaarden, F. L. Moll, F. Auricchio, and S. Trimarchi. An experimental investigation of the impact of thoracic endovascular aortic repair on longitudinal strain. *Eur. J. Cardiothorac. Surg*. 50:955–961, 2016.

[32]Nietlispach, F., N. Wijesinghe, R. Gurvitch, E. Tay, J. P. Carpenter, C. Burns, D. A. Wood, and J. G. Webb. An embolic deflection device for aortic valve interventions. *JACC Cardiovasc. Interv*. 3:1133–1138, 2010.

[33]Nuis, R. J., N. M. Van Mieghem, C. J. Schultz, A. Moelker, R. M. van der Boon, R. J. van Geuns, A. van der Lugt, P. W. Serruys, J. Rodés-Cabau, R. T. van Domburg, and P. J. Koudstaal. Frequency and causes of stroke during or after transcatheter aortic valve implantation. *Am. J. Cardiol*. 109:1637–1643, 2012.

[34]Osnabrugge, R. L., D. Mylotte, S. J. Head, N. M. Van Mieghem, V. T. Nkomo, C. M. LeReun, A. J. Bogers, N. Piazza, and A. P. Kappetein. Aortic stenosis in the elderly: disease prevalence and number of candidates for transcatheter aortic valve replacement: a meta-analysis and modeling study. *J. Am. Coll. Cardiol*. 62:1002–1012, 2013.

[35]Passerini, T., A. Quaini, U. Villa, A. Veneziani, and S. Canic. Validation of an open source framework for the simulation of blood flow in rigid and deformable vessels. *Int. J. Numer. Methods Biomed. Eng*. 29(11):1192–1213, 2013.

[36]Quarteroni, A., R. Sacco, and F. Saleri. Numerical Mathematics. New York: Springer, 2010.

[37]Raghav, V., S. Sastry, and N. Saikrishnan. Experimental assessment of flow fields associated with heart valve prostheses using particle image velocimetry (PIV): recommendations for best practices. *Cardiovasc. Eng. Technol*. 12:1–5, 2018.

[38]Rodés-Cabau, J., P. Kahlert, F. J. Neumann, G. Schymik, J. G. Webb, P. Amarenco, T. Brott, Z. Garami, G. Gerosa, T. Lefèvre, and B. Plicht. Feasibility and exploratory efficacy evaluation of the Embrella Embolic Deflector system for the prevention of cerebral emboli in patients undergoing transcatheter aortic valve replacement: the PROTAVI-C pilot study. *JACC Cardiovasc. Interv*. 7:1146–1155, 2014.

[39]Rodés-Cabau, J., and R. Puri. Filtering the truth behind cerebral embolization during transcatheter aortic valve replacement. *JACC Cardiovasc. Interv*. 8:725–727, 2015.

[40]Saad, Y., and M. H. Schultz. GMRES: a generalized minimal residual algorithm for solving nonsymmetric linear systems. *SIAM J. Sci. Stat Comput*. 7(3):856–869, 1986.

[41]Shadden, S. C., and A. Arzani. Lagrangian postprocessing of computational hemodynamics. *Ann. Biomed. Eng*. 43(1):41–58, 2015.

[42]Stortecky, S., S. Windecker, T. Pilgrim, D. H. Heg, L. Buellesfeld, A. A. Khattab, C. Huber, S. Gloekler, F. Nietlispach, H. Mattle, and P. Jüni. Cerebrovascular accidents complicating transcatheter aortic valve implantation: frequency, timing and impact on outcomes. *EuroIntervention*. 8:62–70, 2012.

[43]Tse, K. M., R. Chang, H. P. Lee, S. P. Lim, S. K. Venkatesh, and P. Ho. A computational fluid dynamics study on geometrical influence of the aorta on haemodynamics. *Eur. J. Cardiothorac. Surg*. 43(4):829–838, 2012.

[44]Vahanian, A., O. R. Alfieri, N. Al-Attar, M. J. Antunes, J. Bax, B. Cormier, A. Cribier, P. De Jaegere, G. Fournial, A. P. Kappetein, and J. Kovac. Transcatheter valve implantation for patients with aortic stenosis: a position statement from the European Association of Cardio-Thoracic Surgery (EACTS) and the European Society of Cardiology (ESC), in collaboration with the European Association of Percutaneous Cardiovascular Interventions (EAPCI). *Eur. J. Cardiothorac. Surg*. 34:1–8, 2008.

[45]Van Mieghem, N. M., N. El Faquir, Z. Rahhab, R. Rodríguez-Olivares, J. Wilschut, M. Ouhlous, T. W. Galema, M. L. Geleijnse, A. P. Kappetein, M. E. Schipper, and P. P. de Jaegere. Incidence and predictors of debris embolizing to the brain during transcatheter aortic valve implantation. *JACC Cardiovasc. Interv*. 8:718–724, 2015.

[46]Van Mieghem, N. M., M. E. Schipper, E. Ladich, E. Faqiri, R. van der Boon, A. Randjgari, C. Schultz, A. Moelker, R. J. van Geuns, F. Otsuka, and P. W. Serruys. Histopathology of embolic debris captured during transcatheter aortic valve replacement. *Circulation* 127(22):2194–2201, 2013.

[47]Webb, J. G., L. Altwegg, R. H. Boone, A. Cheung, J. Ye, S. Lichtenstein, M. Lee, J. B. Masson, C. Thompson, R. Moss, and R. Carere. Transcatheter aortic valve implantation. *Circulation* 119:3009–3016, 2009.

[48]Webb, J. G., S. Pasupati, L. Achtem, and C. R. Thompson. Rapid pacing to facilitate transcatheter prosthetic heart valve implantation. *Catheter. Cardiovasc. Interv*. 68(2):199–204, 2006.

[49]Werner, N., U. Zeymer, S. Schneider, T. Bauer, U. Gerckens, A. Linke, C. Hamm, H. Sievert, H. Eggebrecht, and R. Zahn. Incidence and clinical impact of stroke complicating transcatheter aortic valve implantation: results from the German TAVI registry. *Catheter. Cardiovasc. Interv*. 88:644–653, 2016.

[50]Zahn, R., U. Gerckens, A. Linke, H. Sievert, P. Kahlert, R. Hambrecht, S. Sack, M. Abdel-Wahab, E. Hoffmann, R. Schiele, and S. Schneider. Predictors of one-year mortality after transcatheter aortic valve implantation for severe symptomatic aortic stenosis. *Am. J. Cardiol*. 112:272–279, 2013.